Mine Water and the Environment (2021) 40:366–377
https://doi.org/10.1007/s10230-020-00743-1

TECHNICAL ARTICLE

Mechanism of Water Inrush of a Deep Mining Floor Based on Coupled Mining Pressure and Confined Pressure

Yujun Zhang[1,2]

Received: 26 April 2020 / Accepted: 19 November 2020 / Published online: 5 January 2021

Abstract

We studied the water inrush mechanism in deep mines using experiments to determine the full stress–strain permeability of different lithologies in deep coal seam floors. We also performed numerical simulations of rock floor failure and confined water uplift variation, fracture evolution, permeability variations of coal seam floor failure, and monitored confined water uplift. The results show that water inrush is related to the coupling of mining pressure and water pressure, which expand after unloading, similar to the way rocks soften in stress–strain permeability experiments after peak stress. This conclusion has been confirmed by field drilling, water injection tests, and numerical simulations. The water-bearing layer of the floor strata can be modified (strengthened) by grouting to reduce confined water flow. Technical measures can be taken to divert pressure from and reduce damage to the floor strata and thereby prevent water inrush through the coal floor.

Keywords Confined aquifer · Fluid–solid coupling · Seepage failure · Confined water uplift

Introduction

Water pressure and bottom slab disturbances increase with mining depth mining intensity, which exacerbates the damage and severity of potential water inrush accidents. Water inrush accidents in deep coal mine floors remain poorly understood and a systematic method to effectively predict and prevent their occurrence is needed. Previous studies of water inrush through the mine floor have proposed a variety of criteria and theories (e.g. Slyssalioff formula, water inrush coefficient method, lower three zones, and zero position failure theory; Wang and Liu 1993; Wu 2014; Xie et al. 2012), which have helped prevent water inrush through coal mine floors. Predicting the likelihood of such an event has been attempted using computational methods, probability, main control, and vulnerability indexes, pan-decision theory, geographic information systems, and neural network, expert system, multi-source information composite processing, support vector machine methods, and nonlinear theory methods (Jin 2000; Jiang et al. 1999; Liu and Chen 2001; Liu and Tang 2001; Shi et al. 2015; Wang and Song 2001; Wu and Zhang 2007; Wu et al. 2013; Yan et al. 2008; Zhang and Xue 2009). Nevertheless, industrial field tests remain limited because of the destructive and sudden nature of water inrush accidents in highly confined aquifers.

Feng et al. (2006) used a self-developed seepage and stress-coupling analysis system to simulate the process of fracture instability in a confined water floor. Xu (2011) considered bottom plate (the floor strata) bearing pressure conditions > 5 MPa, collected a large amount of water inrush data as background, and analyzed the formation and influential factors of water inrush events including water–rock interaction, space–time distribution, and bottom plate behavior. Sun et al. (2016) analyzed the formation mechanism of a water inrush channel in an intact high-pressure water bottom plate, and developed a similar material for simulating solid-current coupling and deep water inrush to determine the fracture evolution characteristics of the underlying rock layer. On the basis of subtle rock damage fracture characteristics, Lu and Wang (2015) used Comsol numerical simulation software to simulate and analyze water inrush channels.

These results appropriately represent the role of the aquifer, ground pressure, water pressure and, coal-rock structure in determining the water inrush mechanism. Nevertheless, water inrush from a coal mine floor is a geological

✉ Yujun Zhang
53325605@qq.com

[1] Department of Coal Mining and Designing, Tiandi Science and Technology Co., Ltd, Beijing 100013, China

[2] State Key Laboratory of Coal Mining and Clean Utilization, China Coal Research Institute, Beijing 100013, China

engineering problem related to groundwater mechanics and is related to crack initiation, propagation, and penetration of rock strata driven by mine pressure and water pressure until the final fracture leads to an unstable rupture. An important aspect of study therefore involves the seepage failure characteristics of bottom rock mass under the influence of pressure, especially with regards to fracture evolution under solid-flow coupling, mass deformation, and damage. The geological conditions of a coal mine in Fengfeng, China were used to identify the mechanism of deep mining floor water inrush based on the combined action of mining and confined water pressure. The results provide guidance for water inrush risk prediction and control practices.

Materials and Methods

Starting Material

We selected coarse sandstone, medium sandstone, mudstone, and fine sandstone from the Fengfeng mining area for infiltration tests. Specimens were prepared into square columns with dimensions of 50 × 50 × 100 mm. After depressurizing an evacuated vacuum tank for 24 h, the prepared specimen was injected into the tank using negative pressure to cause the specimen to reach its water saturation state. Figure 1 shows the prepared standard specimen and post-packaged specimen.

Experimental Protocol

We used the pressure relief loading method in which a servo press and four high-pressure oil cylinders act together to apply a controllable axial load. A high-pressure nitrogen source was used to drive the water to provide a stable osmotic pore pressure, which was controlled and maintained by a regulation valve. A manual pump was used to generate the confining pressure, which was stabilized by an energy storage tank. Real-time data were collected from pressure and displacement sensors, and the water flow rate was measured by the mass method. Figure 2 shows a schematic diagram of the basic principle of the penetration tests; in each test, we applied a certain axial pressure p_1, confining pressure p_2, and pore pressure p_3 ($p_3 < p_2$), and then reduced the pore pressure at one end of the specimen to p_4 to form an osmotic pressure difference at both ends of the specimen ($Dp = p_3 - p_4$), thus causing water to pass through the specimen. The change of axial deformation and osmotic pressure difference with time was recorded throughout the entire test. Stress–strain-permeability curves were obtained according

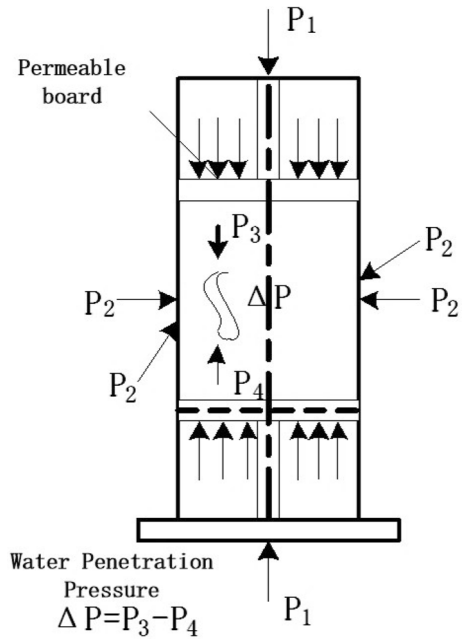

Fig. 2 Basic principles of the penetration tests:

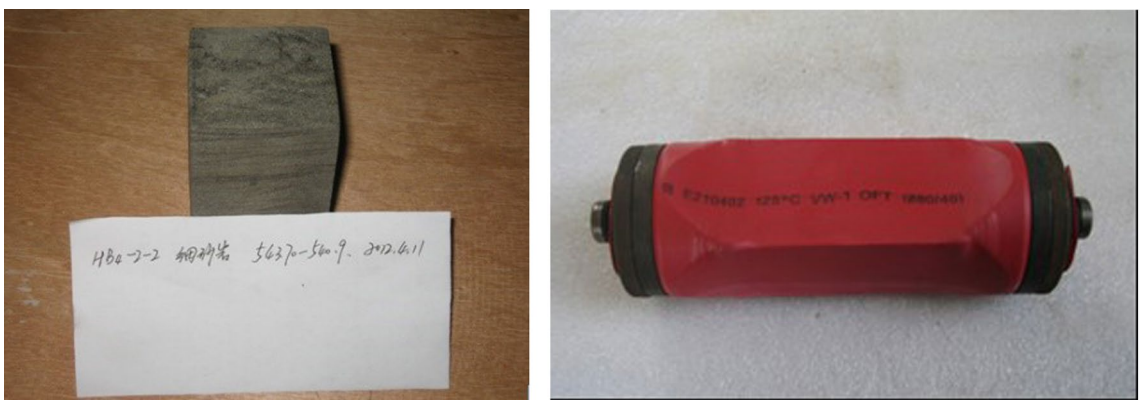

Fig. 1 Standard prepared specimen (left) and post-packaged specimen (right)

to the strain and permeability data at each axial pressure stage.

Experimental Results

Figure 3 shows the specimen morphology after loading failure. The failure mode is mainly characterized by a combination of tensile splitting and shear failure, in which the former dominates. Spalling sheets are observed on the specimen surface, particularly the failure surface with steeper angles, and are primarily developed along the original fracture extension. Figure 4 shows the stress–strain-permeability curves of the different lithologies. The results show that the total stress–strain permeability curves essentially undergo five different processes: initial fracture; compaction-elastic; deformation-yield; failure-strain; and softening-residue strength. The permeability of mudstone does not appear

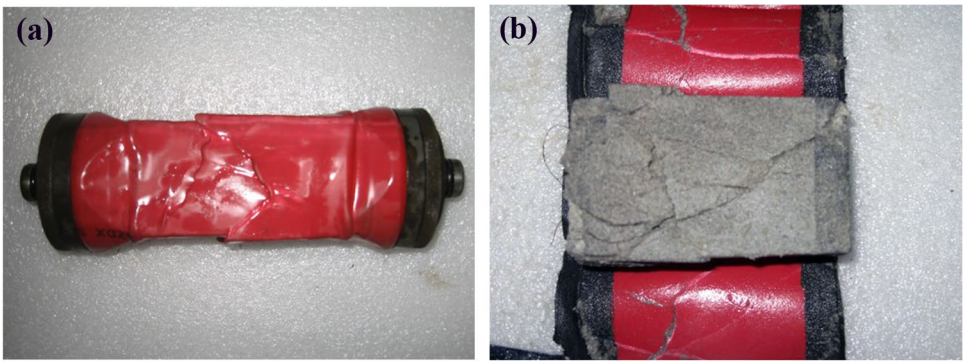

Fig. 3 Specimen failure morphology after loading **a** destruction of appearance; **b** split destruction

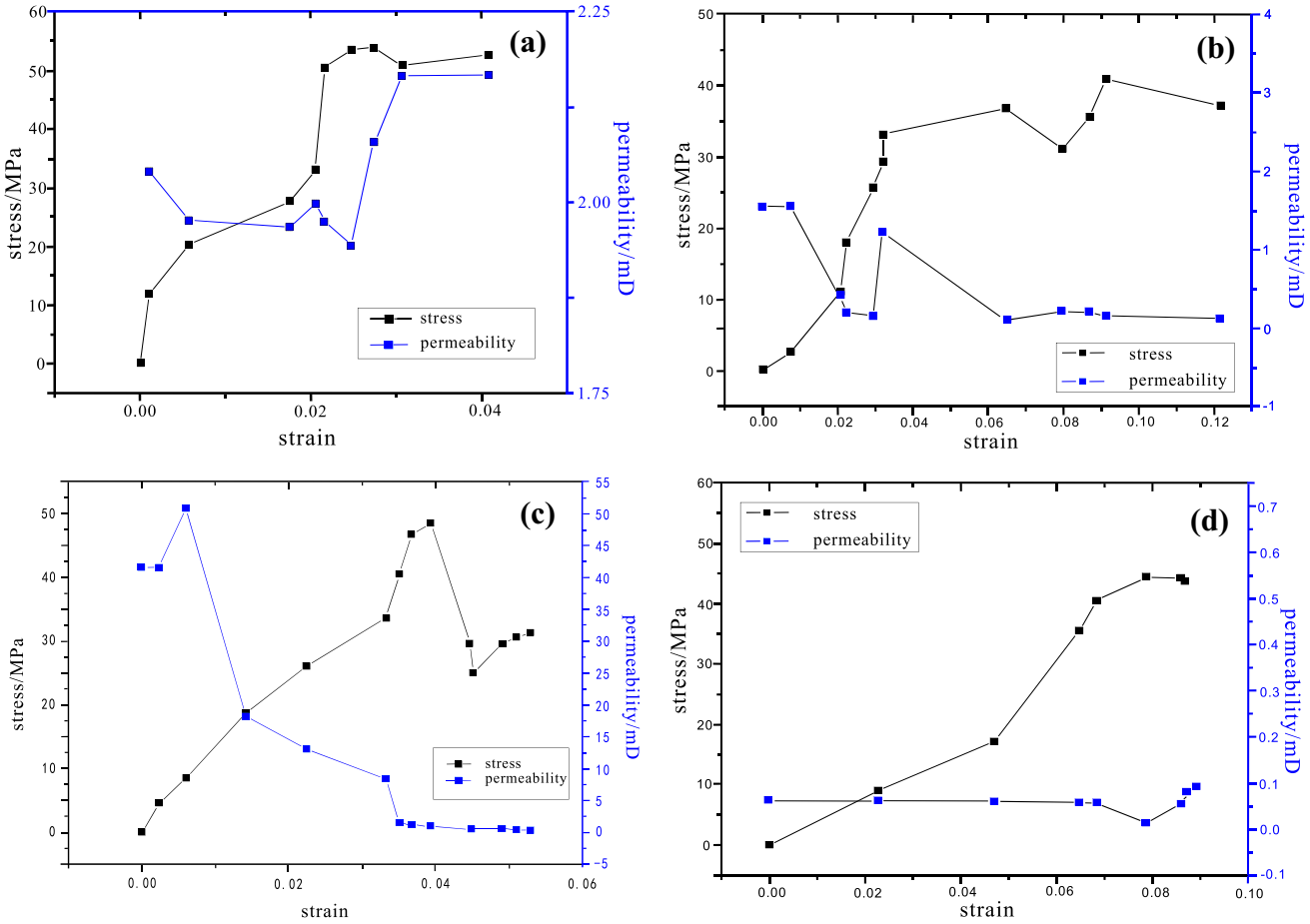

Fig. 4 Stress–strain-permeability curves **a** middle sandstone; **b** fine sandstone; **c** grit stone; **d** mudstone

to change prior to reaching the peak rock strength and then decreases slowly with increasing stress. An abrupt increase of permeability is observed after the stress–strain curve peak. Sandstone's high porosity is the main reason it is so permeable prior to loading. With increasing stress, the cracks and pores of each specimen are compressed and close, and permeability gradually decreases. The permeability of coarse sandstone decreases with strain. The change of permeability in different stress stages after the peak is closely related to the original rock porosity and state of fracture development. However, in both sandstone and mudstone, peak permeability generally occurs during the strain-softening stage. After attaining peak strength, the failure surface begins to stagger, the degree of crack opening and penetration increase continuously with increasing strain, and the permeability reaches a peak with crack expansion. This demonstrates that rock failure is not synchronized with maximum permeability, but that further deformation after failure leads to the appearance of peak permeability.

Numerical Simulations

Model Establishment

The flow-solid coupling function module in FLAC3D software is based on two-field coupling in a porous media percolation model realized by Biot osmotic consolidation theory. A function that considers the coupling effect of seepage stress parameters was established by applying the built-in FISH language for secondary development, so that the permeability coefficient can be adjusted with changing stress and coupling of seepage stress parameters can be achieved in the double-field coupling numerical simulation calculations.

We designed the model on the basis of the engineering geological conditions of a mine in the Fengfeng area. The average burial depth of the working face was 636 m, the average coal seam thickness was 4.2 m, the average inclined coal and rock layer angle was 20°, the slope length of the working face was 170 m, the head pressure was > 5 MPa, the simulated working face length was 110 m, and the propulsion length was 150 m. To eliminate the boundary effect, we used a boundary width of 150 m in the vertical direction, and similar lithologies were merged, with each layer selected according to its actual thickness. After simplification, the model length was 450 m, the width was 450 m, and the vertical height was 150 m. The numerical model is shown in Fig. 5.

A horizontal constraint was applied to the front and left boundaries of the calculation model, that is, the horizontal displacement of the boundary and the horizontal and vertical displacement of the bottom boundary were all set to zero; the top was a free boundary. An equivalent load was applied (i.e. deadweight stress). Given the impervious boundary around the model, the excavated section was regarded as impervious and the initial pore water pressure was given at the left and right boundaries. The pore water pressure corresponds to the linear variation of different water level conditions according to the hydraulic gradient. The Mohr–Coulomb yield criterion was used for mechanical analysis and Darcy's law for seepage analysis (assuming the floor was porous). The mechanical and hydraulic parameters of each coal stratum in the model are listed in Table 1.

Analysis of Simulation Results

Failure and Confined Water Uplift of the Floor

From the failure field and the confined water vector field, we obtain the process and position of rock fracture development, penetration, confined water uplift, and water inrush under the combined action of mining and water

Fig.5 Three-dimensional model

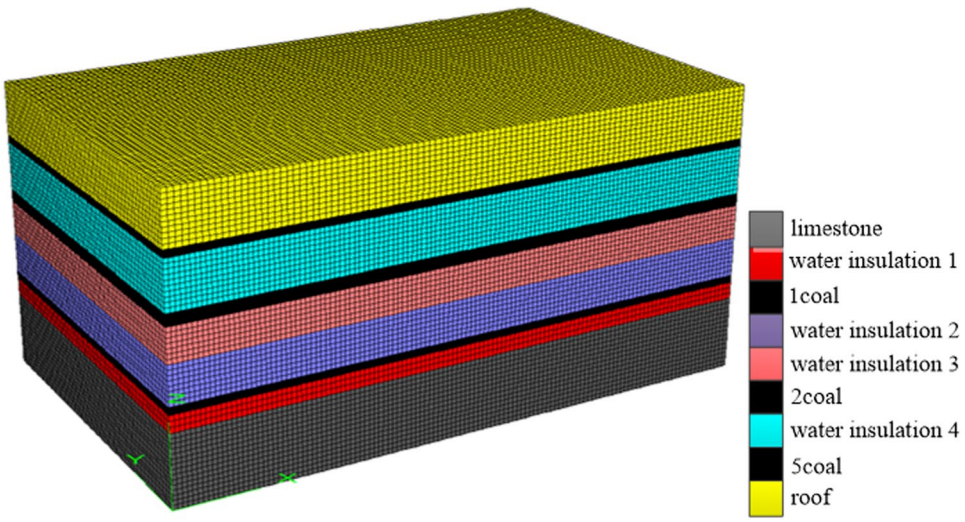

Table 1 Rock mechanical parameters

Rock	Uniaxial pressure strength (MPa)	Elasticity modulus (MPa)	Deformation modulus (MPa)	Cohesion (MPa)	Internal friction angle	Volume modulus of fluid (GPa)	Porosity	Osmotic coefficient (m^2/Pa.s)	Density (kg/m^3)
Siltite	18.1	2000	2469	1.2	36	2.0	0.05	10e – 12	2700
Med. ss	12.03	2021.5	2222.0	1.0	14.0 ~ 32.6	2.0	0.05	10e – 12	2700
Ms	30.0	1161.3	1840.0	2.50	27.1	2.0	0.05	10e – 12	2700
#2 Coal	10	1000	520	0.05	18	2.0	0.15	10e – 12	1520
Fine ss	18.6	1500	1006.8	1.2	25	2.0	0.05	10e – 12	2700
Siltite	30.2	1519.9	2669.8	2.5	25.8	2.0	0.05	10e – 12	2700
Ms	18	1800	2000	1.0	30	2.0	0.05	10e – 12	2700
Ls	100	2500	2200	3.2	32	2.0	0.3	10e – 11	2720

ss sandstone, *ms* mudstone, *ls* limestone

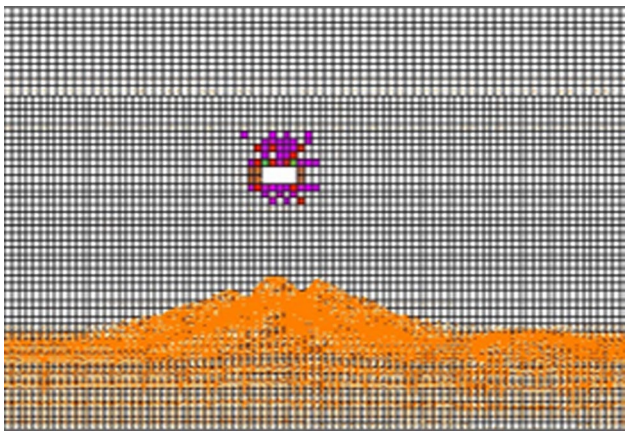

Fig. 6 The 30 m roof, floor damage, and pressure water lift height

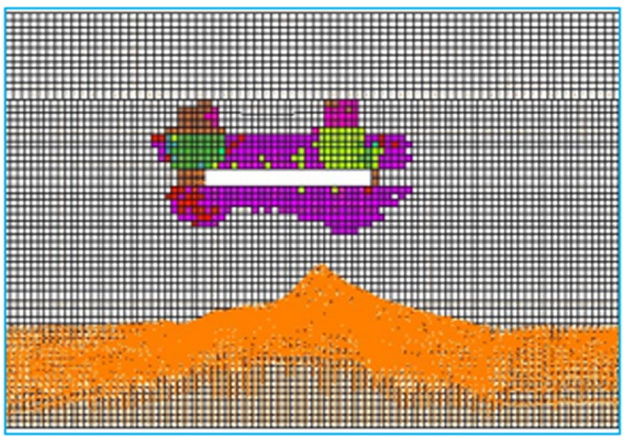

Fig. 7 The 90 m roof, floor damage, and pressure water lift height

pressure. Figures 6 and 7 show the results of mining failure on the floor strata and the characteristics of confined water uplift under different propulsion lengths in the working face. When mining begins, plastic damage occurs in the aquiclude in the floor strata, and the damaged area of the coal seam floor gradually increases. As the working face advances less than 30 m (initial pressure), the damaged area of that aquiclude is small, generally within 9 m. When the working face advances to ≈ 50 m after two periods of pressure (≈ 10 m apart), the development depth and range of the plastic area of the floor rock rapidly develops to 18 m and the failure form is essentially compression-shear failure. As the working face advances to ≈90 m, the floor damage gradually stabilizes, the depth no longer increases, and the maximum depth reaches 21 m. The original uplift zone height at the upper aquifer boundary is given from the confined water prior to mining of the working face. Because of the homogenization treatment of the rock strata during the simulations and absence of original fissures, the development top of the original uplift zone is relatively ordered with a height of ≈ 3 m. As the working face advances, the flow path state of the bottom aquifer initially changes, reflecting the flow state toward the goaf. Under the combined action of mining pressure and water pressure, the confined water continues to press upward on the basis of the original lifting belt, which reduces the thickness of the effective water barrier. The development of floor strata failure and rise of confined water are closely related to the initial pressure and periodic pressure increases at the roof.

Figure 8 shows the simulated results of floor failure and confined water uplift distribution due to mining. Similar to previous studies, the bottom rock mass between the coal seam and aquifer is divided into four zones from top to bottom according to its failure characteristics, in which the third zone is the height of the confined water that continues to be guided by the coupling of water pressure and mineral compaction. This can be referred to as the confined water solid–fluid coupling uplift zone.

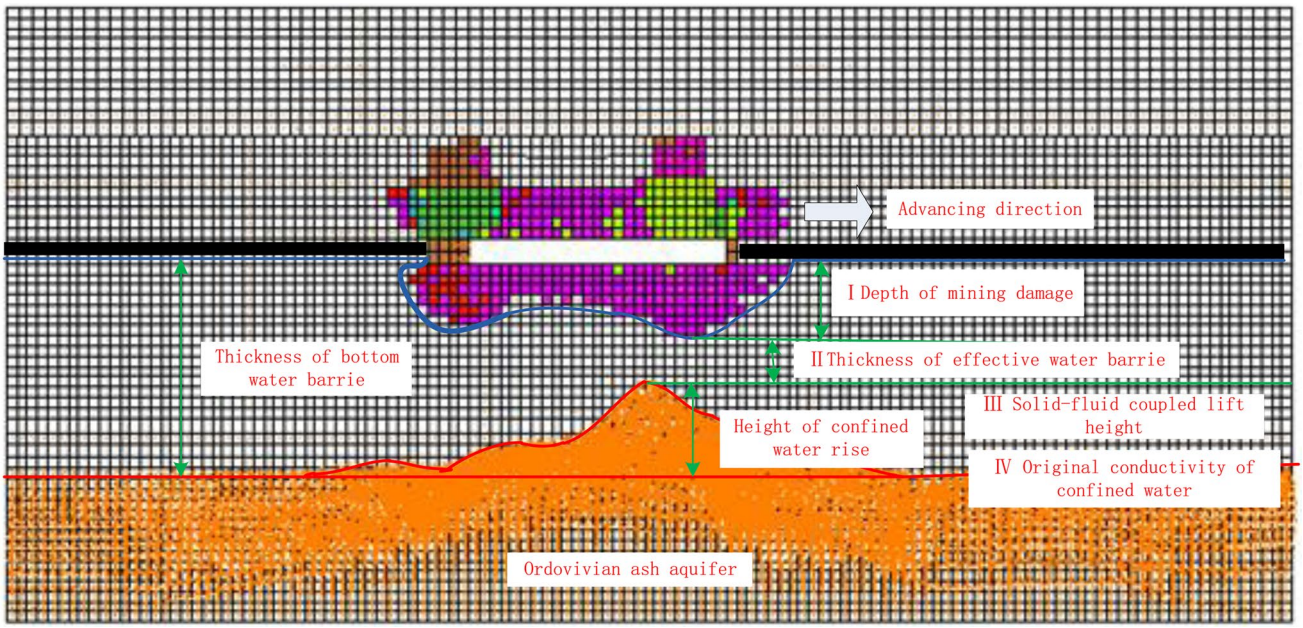

Fig. 8 Chart of the four floor damage zones

Water Inrush of the Bottom Plate

To further simulate the water inrush process and position under the combined action of mineral and water pressures, we connected the depth of mining failure with the height of the confined water conduction belt by reducing the thickness of the floor strata aquiclude to 25 m. Figures 9 and 10 show the simulated results of the maximum main stress field of the coal seam floor and seepage field of confined water. As the working face advances to 30 m, the confined water is guided upward under the joint action of mining and water pressure but does not form a water channel into the floor

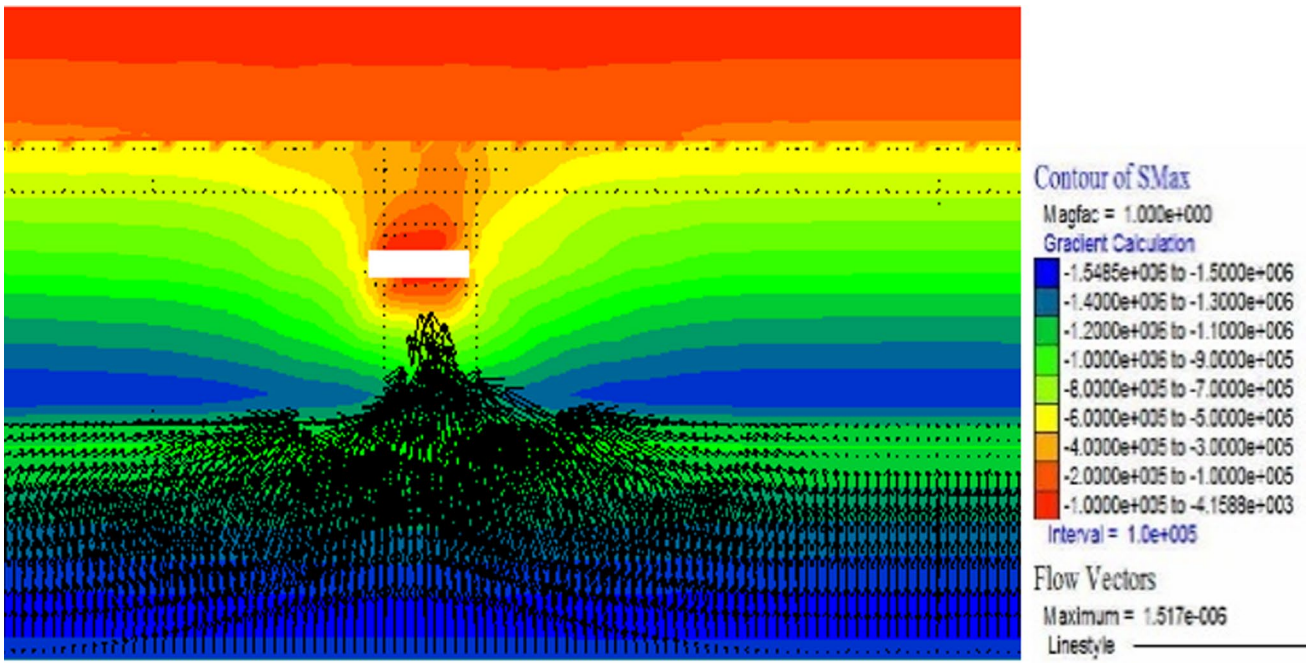

Fig. 9 Water-conduction passage for the bottom plate when the working face advances to 30 m

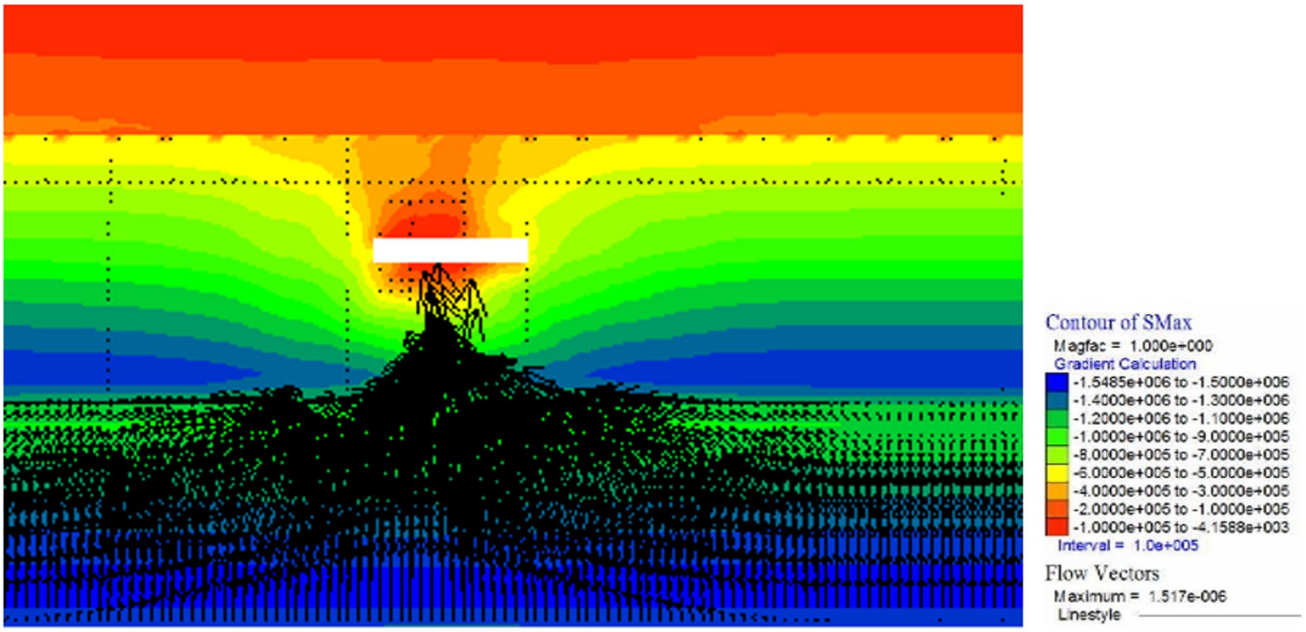

Fig. 10 Water inrush from the floor when the face advances to 40 m)

strata failure zone. As the working face advances to 40 m, under the action of roof pressure, the confined water rapidly ascends and reaches this failure zone. At this point, the flow vector path points to the goaf, and water inrush occurs. The failure zone and confined water solid flow form the main water inrush channel.

Dynamic Monitoring of Coal Seam Floor Failure and Confined Water Uplift

Monitoring Scheme and Drilling Arrangement

We used the 112,145 working face of the Fengfeng mine as a testing location. A borehole stress meter and borehole peep were used to measure the failure depth and fracture evolution of the deep mining floor. Four boreholes were located 27.1 m from the open hole of the working face, of which three were water injection test boreholes. The overall control depth was 18.17–28.71 m, and the control depth was 9.53–24.53 m for one stress–strain test hole. The main drilling construction parameters are listed in Table 2.

Monitoring Results Analysis

Measured Results of Borehole Water Injection Test

The variation and relative variation of the permeability coefficient before and after mining were determined based on the water injection test parameters λ to assess the failure depth of the floor strata. Assuming that the permeability coefficient of rock mass prior to mining is a certain value, the failure depth of coal seam floor affected by mining is assessed by:

$$\Delta K^* = K_2^* - K_1^* = \alpha \frac{Q_2 - Q_1}{L^* P^*}, \quad (1)$$

where DK^* is the increment of the rock permeability coefficient at a certain depth (m/d), K_1^* and K_2^* are the permeability coefficients of the rock prior to and after mining (m/d),

Table 2 Main parameters of floor failure depth test hole construction

No.	Design vertical depth (m)	True vertical depth (m)	Actual borehole inclination (°)	Drilling azimuth (°)	Test method
1#	29	28.71	− 69	284	Water injection test + camera shooting
2#	23	24.36	− 68	284	Water injection test
3#	27	24.5	− 68	284	Stress–strain tester
4#	17	18.19	− 63	284	Water injection test

respectively, α- coefficient, Between 0.83 ~ 1.18, L^*Length of water injection section (m),P^* Water pressure (MPa), and Q_1 and Q_2 represent the infiltration water injection prior to and after mining (m^3/d), respectively. We set K_1^* to zero and when D$K^* \geq 0.2$ m/d, the rock mass of the floor strata was considered destroyed.

Figure 11 shows the relationship between the change of permeability coefficient of the no. 1 and 2 boreholes and their distances from the working face. Figure 11a shows that the floor strata reaches the penetration failure criterion when the working face advances to 18.6 m; the maximum is reached when the working face reaches 21 m, followed by a gradual decrease, and a small fluctuating increase occurs once the working face reaches 27.5 m. Figure 11b shows that when the working face advances to 3.6 m, the rock mass abruptly unloads from the increasing stress state, resulting in a certain degree of floor strata damage and partial mining cracks, which weaken the permeability of the bottom rock mass. As the working face pushes through the borehole to 15.8 m, the coal seam floor is in the goaf and outside the range of slip deformation failure, the coal seam roof collapse range decreases, and the floor penetration failure reaches its maximum. Over the range of 15.8–24.7 m, the fractures gradually recover but the permeability coefficient of the coal seam floor remains unchanged. When the coal face reaches 24.7–30.9 m, the permeability coefficient of the floor responds because the roof collapse compacts again and a stress disturbance to the floor rock is produced. This verifies that the rock permeability in the laboratory test gradually increases and reaches its peak during the unloading of the plastic stage. The borehole water injection analysis shows that the failure depth occurs between 18.2 and 24.3 m.

Elevation Height of the Compressed Water

Effluent was observed at a burial depth of 25.3 m during construction of the no.1 borehole, about 13 m from the top interface of the Ordovician aquifer. Under the joint action of mining pressure and confined water, the confined water surged upward to form a pressure-induced uplift, but did not reach the depth of the bottom plate failure.

Borehole Data from the Stress–Strain Tests

Four stress–strain gauges were arranged at different depths from the coal seam floor at depths of 9.53, 13.82, 20.24, and 24.3 m. Each gauge had four groups of strain gauges, which included two strain gauges distributed vertically. The stress–strain state of the rock mass was demonstrated by the strain increment and accumulative strain variables of the stress strain gauge during mining, which provides a reference for determining the failure depth of the coal seam floor.

Figure 12a shows that the maximum strain increment of stress gauge #1 when the working face was 12 m from the gauge, all of the strain changes of the coal seam floor were negative, which implies that the rock underwent deformation and destruction and did not return to its original stress state. Figure 12b shows that the channel strains decreased monotonically as the working face advanced, which is indicative of irreversible plastic deformation failure. Figure 12c shows that when the working face propulsion distance was 10–12 m from stress–strain gauge #4, the strain state of the coal seam floor changed substantially. Figure 12d shows that after the working face pushed through the borehole, the rock was in an elastic state and did not reach the plastic yield limit. In summary,

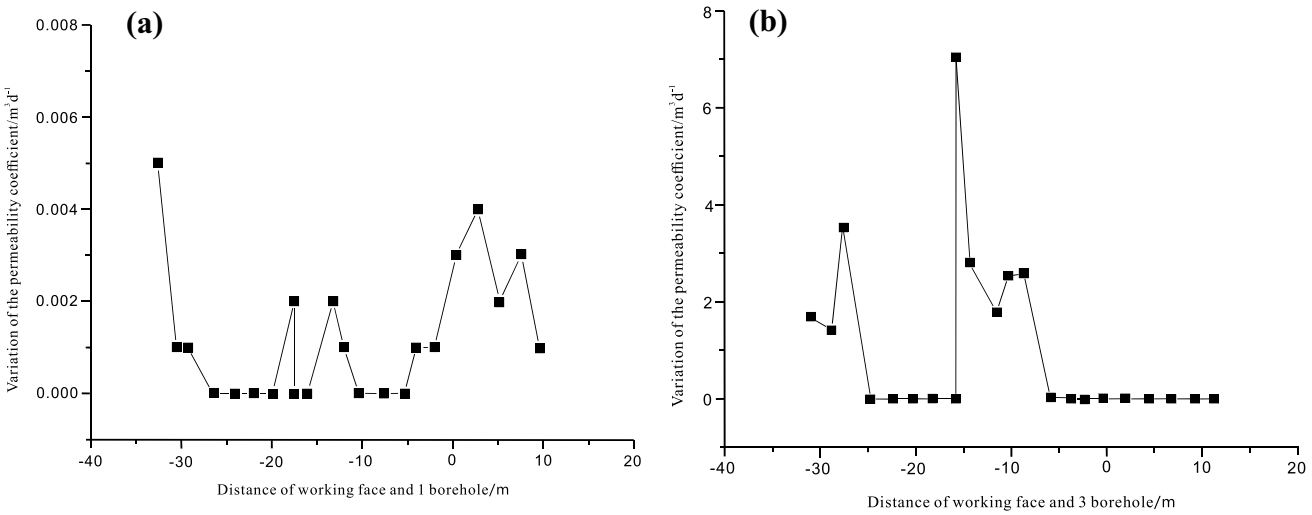

Fig. 11 Variation of the permeability coefficient of the water injection hole of the floor as a function of distance from the panel: **a** Strain increment, **b** cumulative variation in strain, **c** strain increment, **d** cumulative variation in strain

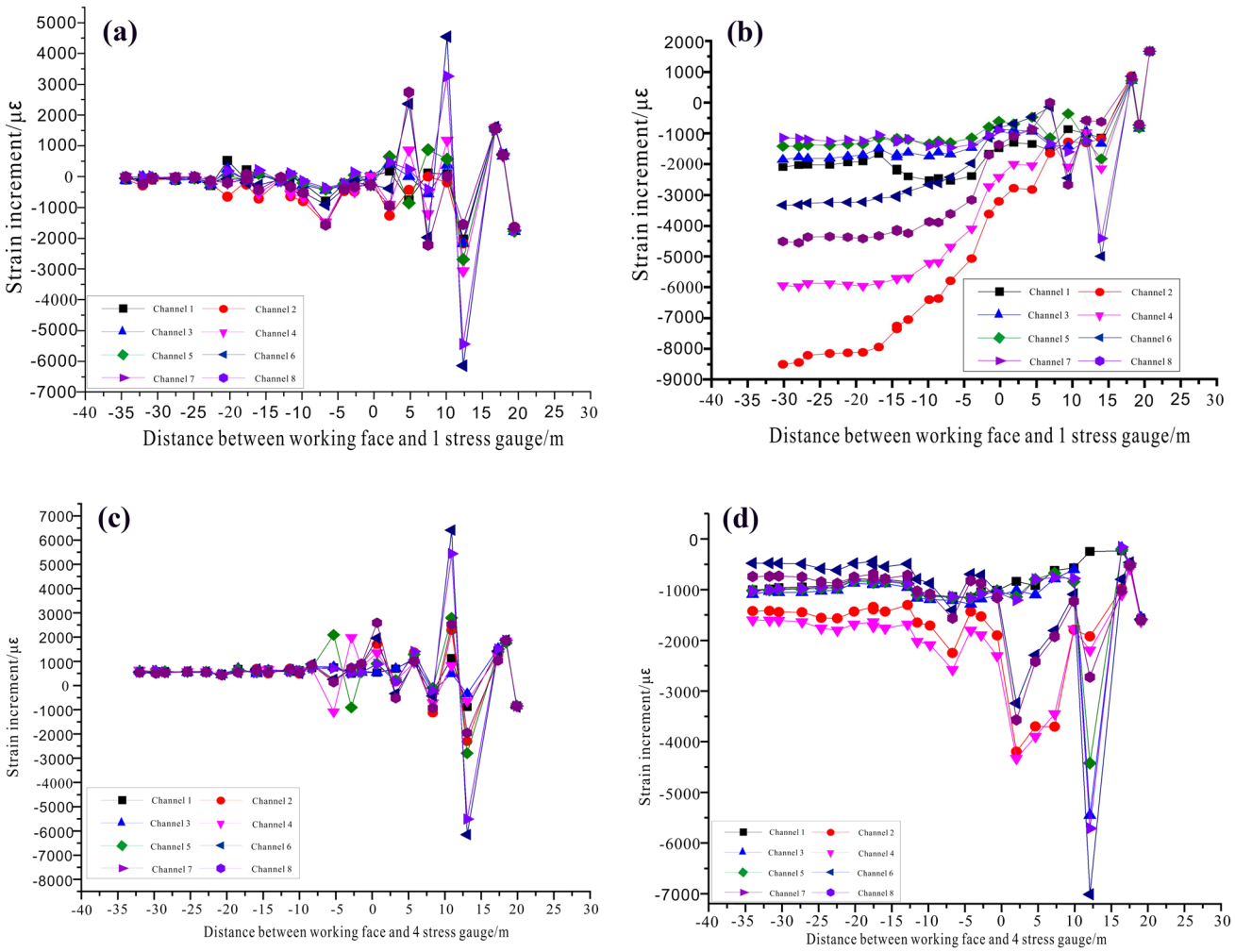

Fig. 12 Variation curves of stress–strain gauge #1 (**a**, **b**) and #4 (**c**, **d**) with distance from the panel

the stress–strain analysis shows that the peak value of the leading support pressure was 10–12 m in front of the working face; the failure depth of the coal seam floor was 13.8–20.2 m.

Penetration Results of Fracture Evolution

Figure 13 shows the peep results at different depths of borehole 1. At a depth of 5.6 m, the borehole wall had bedding crack deformation and at 15.6 m, disturbance is visible yet minor, with mainly transverse fissures. At 17.7 m, there is

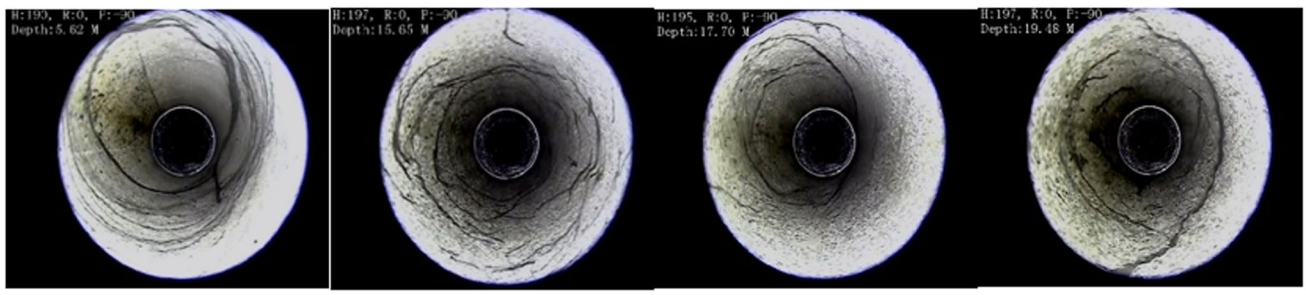

Fig. 13 Evolution of fractures in the bottom strata during coal seam mining

clear dislocation and longitudinal fissuring, which reflects severe post-harvest pressure relief disturbance failure characteristics. At 19.5 m, the number of cracks visibly decreases and the mining disturbance gradually weakens, which is roughly consistent with the no. 1 hole injection test results.

Damage Depth of the Floor and Elevation of the Confined Water

The results of the monitoring data analysis from the three methods above show that the bottom rock strata in the control depth of coal seam floor drilling in this working face are damaged to different degrees under the combined action of mining and confined water pressure. The maximum measured damage depth of the bottom slab was 24.3 m and the guiding height of the confined water was ≈ 13 m.

Water Inrush Mechanism

The total stress–strain permeability test results show that the peak rock permeability generally occurs in the stress-softening stage after rock failure (section DE in Fig. 14). At this time, the failure surface after peak strength begins to stagger, crack opening and penetration increase with increasing strain, and the permeability reaches a maximum with crack expansion during failure. The extended penetration of rock axial fractures is therefore a necessary condition for the increased permeability.

The numerical simulations and field measurements show that permeability is generally low when the rock mass is in its original stress state. During mining, the advance support pressure transferring to the floor strata interacts with the hydrostatic pressure of the confined water. As the working face advances, the goaf space increases and the leading stress compression zone transitions to the pressure relief zone. At this time, the floor strata stress decreases and the bottom plate expands after pressure relief, similar to the softened state after peak stress in the total stress–strain permeability experiments. The occurrence of water inrush is thus due to the process of breaking deformation and sudden permeability changes under the action of mining pressure and water pressure.

Figure 15 is a schematic diagram of the formation and position of the water inrush passage on the bottom plate of the working face. Under the combined action of mining pressure and confined water pressure, the mining water conduction failure zone and solid-current coupling guide belt develop downward and upward, respectively, which decreases the effective aquiclude thickness of the floor strata; the development height is the greatest in the pressure relief zone. The prevention of rock failure and control of further strain softening deformation after rock failure is therefore particularly important for avoiding water inrush. The water-bearing layer of the floor strata can be modified by grouting to reduce the risk of confined water inrush, bypass the ore pressure pathway, and reduce the damage to the bottom plate.

Conclusions

We performed permeability experiments covering all stress and strain conditions of different lithologies in a deep floor mining environment under failure conditions to characterize fracture evolution, in addition to numerical simulations and

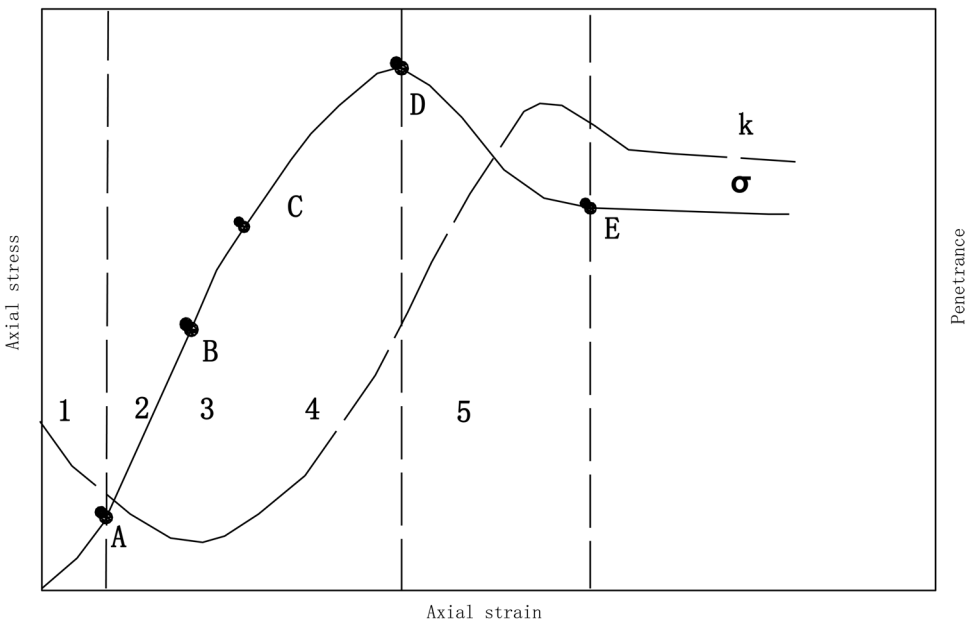

Fig. 14 Schematic diagram of the full stress–strain permeability test

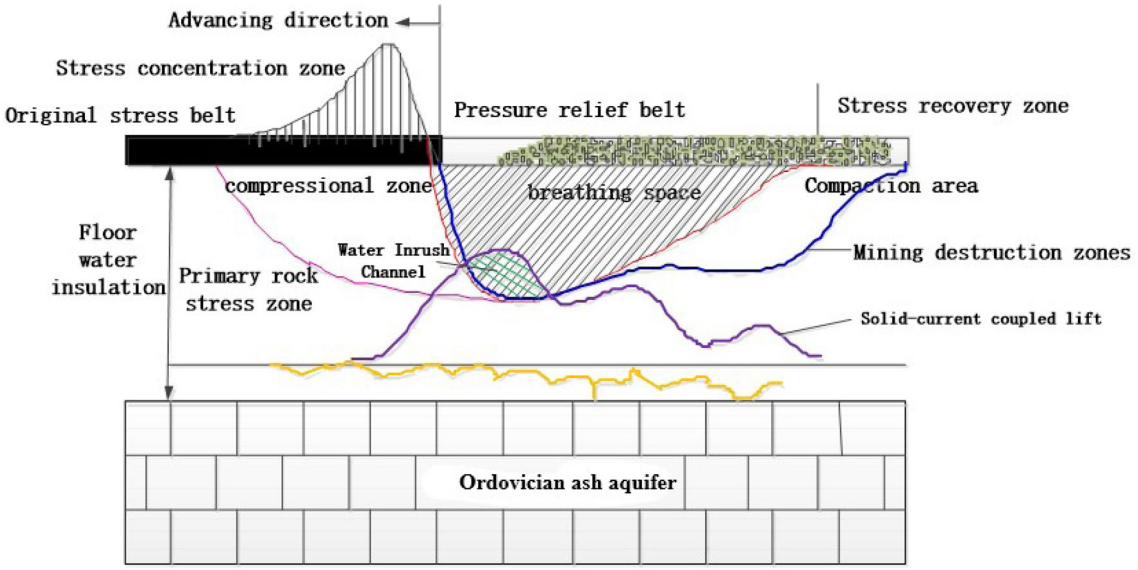

Fig. 15 Formation of water inrush channels

field monitoring of confined water uplift. The main conclusions are:

1. The total stress–strain permeability tests showed that peak rock permeability generally occurs during the stress-softening stage after failure. Fracture opening and penetration degree increase continuously after peak strength with increasing strain and permeability also reaching a maximum. The field drilling water injection test data show that the rock mass of a coal seam floor undergoes fracture expansion and deformation failure owing to mining and unloading, and the penetration failure of the floor reaches a maximum, in agreement with the experimental results.
2. Under the combined action of mining and confined water pressure, the maximum damage depth of the floor strata measured in the field was 24.36 m and the height of the confined water conduction belt was ≈13 m. The numerical simulation indicated that the distribution of confined water uplift was non-linear or wavy, in accordance with the measured results. The main water inrush channel connects the floor strata mining failure zone with the confined water. The occurrence of water inrush through the floor is a response to deformation and permeability changes of the rock mass as the strata breaks under the action of mining and water pressure.
3. Deep coal seam floor water inrush can occur after pressure compression and prior to pressure relief or under unloading during expansion after pressure relief when the penetration failure mutation reaches a maximum. The floor failure zone and confined water–solid-current coupling guide belt interact to form a water channel. This is similar to the softening state after peak stress in stress–strain permeability experiments.
4. To prevent water-inrush disasters, we propose technical measures such as modifying or reinforcing the water-bearing layer of the bottom slab by ground directional drilling regional grouting to reduce the water-conduction of confined water, bypass the pathway of the mining pressure transfer to the floor, and reduce or ameliorate the damage depth of floor strata.

Acknowledgements We thank Fengda Zhang for assistance in revising the figures, Esther Posner, PhD, from Liwen Bianji, Edanz Editing China (www.liwenbianji.cn/ac), for editing the English text of this manuscript, and China's National Natural Science Fund (Grant 51874177)

References

Feng Q, Yang T, Yu Q et al (2006) Numerical simulation on water-inrush from the seam floor based on the coupled analysis of seepage and damage. J Safe Environ 3:1–4 **(in Chinese)**

Jiang D, Wang J, Chen P (1999) Establishment and application of the GIS based forecasting model of floor water bursting in coal mines. Chin J Geol Haz Control 10:67–72 **(in Chinese)**

Jin D (2000) Review on study of Pan*. Decision analysis theory of water inrush forecast through coal bottom layer in mining work face. J Jiaozuo Inst Tech 4:52–56 **(in Chinese)**

Liu W, Chen X (2001) Research of expert system method on floor water-irruption predicting and evaluating. Chin J Geol Haz Control 12(2):7–10 **(in Chinese)**

Liu Y, Tang C (2001) Numerical simulation for the failure process of floor with water pressure. Coal Min Tech 42:50–51

Lu Y-L, Wang L-G (2015) Numerical modeling of time-dependent damage and failure process of rocks based on micro-crack propagation. J China Coal Soc 40(6):1276–1283 **(in Chinese)**

Shi L, Tan X, Wang J, Ji X, Niu C (2015) Risk assessment of water inrush based on PCA- Fuzzy-PSO-SVC. J Chin Coal Soc 1:167–171 **(in Chinese)**

Sun W, Zhang S, Zhu L (2016) Analysis on the formation pattern of water inrush channel in deep mining high pressure water complete floor. Min Safe Environ Prot 43(3):100–102 **(in Chinese)**

Wang Z, Liu H (1993) Coal mining on confined water. China Coal Industry Publishing House, Beijing

Wang L, Song Y (2001) Combined ANN forecast of water-inrush from coal floor. Chin J Geotech Eng 23(4):502–505 **(in Chinese)**

Wu Q (2014) Progress, problems and prospects of prevention and control technology of mine water and reutilization in China. J China Coal Soc 39(5):795–805 **(in Chinese)**

Wu Q, Zhang Z (2007) A new practical methodology of the coal floor water bursting evaluating I—the master controlling index system construction. J China Coal Soc 32(1):42–47 **(in Chinese)**

Wu Q, Zhang B, Zhao W et al (2013) A new practical methodology of coal seam floor water burst evaluation: the comparison study regression among ANN, the weight of evidence and the logistic vulnerable index method based on GIS. Chin J Rock Mech Eng 1:21–26 **(in Chinese)**

Xie H, Zhou H, Xue D (2012) Research and reflection on deep mining and ultimate mining depth of coal. J Coal 37(4):535–542 **(in Chinese)**

Xu Z (2011) Foremasters and prevention of deep mining floor damage and high pressure water inrush mode J. Coal 8:1421–1422 **(in Chinese)**

Yan Z, Bai H, Zhang H (2008) A novel svm model for the analysis and prediction of water inrush from coal mine. China Safe Sci J 18(7):166–170 **(in Chinese)**

Zhang H, Xue G (2009) Prediction of water inrush from coal seam floor confined based on geo-information composite overlay analysis. J China Coal Soc 34(8):1100–1104 **(in Chinese)**